SAND2000-0999J

SPE 57002

Revised for SPE Reservoir Evaluation and Engineering 4/12/00

Heterogeneity, Permeability Patterns, and Permeability Upscaling: Physical Characterization of a Block of Massillon Sandstone Exhibiting Nested Scales of Heterogeneity

Vincent C. Tidwell, SPE, Sandia National Laboratories

John L. Wilson, New Mexico Institute of Mining and Technology

Summary. Over 75,000 permeability measurements were collected from a meter-scale block of Massillon sandstone, characterized by conspicuous cross bedding that forms two distinct nested-scales of heterogeneity. With the aid of a gas minipermeameter, spatially exhaustive fields of permeability data were acquired at each of five different sample supports (i.e., sample volumes) from each block face. These data provide a unique opportunity to physically investigate the relationship between the multi-scale cross-stratified attributes of the sandstone and the corresponding statistical characteristics of the permeability. These data also provide quantitative physical information concerning the permeability upscaling of a complex heterogeneous medium. Here, a portion of the data taken from a single block face cut normal to stratification is analyzed. Results indicate a strong relationship between the calculated summary statistics and the cross-stratified structural features visibly evident in the sandstone sample. Specifically, the permeability fields and semivariograms are characterized by two nested scales of heterogeneity, including a large-scale structure defined by the cross-stratified sets (delineated by distinct bounding surfaces) and a small-scale structure defined by the low-angle cross-stratification within each set. The permeability data also provide clear evidence of upscaling. That is, each calculated summary statistic exhibits distinct and consistent trends with increasing sample support. Among these trends are an increasing mean, decreasing variance, and an increasing semivariogram range. Results also clearly

DISCLAIMER

indicate that the different scales of heterogeneity upscale differently, with the small-scale structure being preferentially filtered from the data while the large-scale structure is preserved. Finally, the statistical and upscaling characteristics of individual cross-stratified sets were found to be very similar owing to their shared depositional environment; however, some differences were noted that are likely the result of minor variations in the sediment load and/or flow conditions between depositional events.

Introduction

Geologic materials are inherently heterogeneous owing to the depositional and diagenetic processes responsible for their formation. These heterogeneities often impose considerable influence on the performance of hydrocarbon bearing reservoirs. Unfortunately, quantitative characterization and integration of reservoir heterogeneity into predictive models is complicated by two challenging problems. First, the quantity of porous media observed and/or sampled is generally a minute faction of the reservoir under investigation. This gives rise to the need for models to predict material characteristics at unsampled locations. The second problem stems from technological constraints that often limit the measurement of material properties to sample supports (sample volumes) much smaller than can be accommodated in current predictive models. This disparity in support requires measured data be averaged or upscaled to yield effective properties at the desired scale of analysis.

The concept of using "soft" geologic information to supplement often sparse "hard" physical data has received considerable attention.[1,2] Successful application of this approach requires that some relationship be established between the difficult to measure material property (e.g., permeability) and that of a more easily observable feature of the geologic material. For example, Davis et al.[3] correlated architectural-element mapping with the geostatistical characteristics of a fluvial/interfluvial formation in central New Mexico; Jordan and Pryor[4] related permeability controls and reservoir productivity to six hierarchical levels of sand heterogeneity in a fluvial meander belt system; while Istok et al.[5] found strong correlation between hydraulic property measurements and visual trends in the degree of welding of ash flow tuffs at Yucca Mountain, Nevada. Phillips and Wilson[6] mapped regions where the permeability exceeds some specified cutoff value and related their dimensions to the correlation length scale by means of threshold-crossing theory. Also, Journal and Alabert[7] proposed a spatial connectivity model based on an indicator formalism and conditioned on geologic maps of observable, spatially connected, high-permeability features.

The description and quantification of heterogeneity is necessarily related to the issue of scale. It is often assumed that geologic heterogeneity is structured according to a discrete and disparate hierarchy of scales. For example, the hierarchical models proposed by Dagan[8] and Haldorsen[9] conveniently classify heterogeneities according to the pore, laboratory, formation, and regional scales. This assumed disparity in scales allows parameter variations occurring at scales smaller than the modeled flow/transport process to be spatially averaged to form effective media properties,[10-14] while large-scale variations are treated as a simple deterministic trend.[2,15] However, natural media are not always characterized by a large disparity in scales as assumed above;[16] but rather, an infinite number of scales may coexist[17-20] leading to a fractal geometry or continuous hierarchy of scales.[21]

Clastic sedimentary formations have long been described in terms of the hierarchy of bedforms specific to a particular depositonal environment. The hierarchical bedform assemblages largely dictate the spatial permeability patterns characterizing these formations. Two empirical examples include the Page sandstone, an eolian deposit,[22,23] and the Rannoch Formation, a storm-dominated shoreface sandstone.[24] Experimental observation[25] and numerical studies[26-28] suggest that even the smallest-scale heterogeneities can significantly influence flow and transport processes for a number of important engineering problems. Representing small-scale structure in upscaled parameters is complicated by the tendency of the bedforms to vary in size, shape, and orientation across the hierarchy of scales. For this reason, the computation of grid-block permeabilities is commonly approached numerically as the output of fine-scale simulations. This process is performed in a step-wise manner starting at the smallest scale of heterogeneity and progressing from one discrete scale of heterogeneity to the next until the desired scale of analysis is achieved. This is referred to as upscaling by grid-block averaging[29] or psuedofunctions.[30-32] Kasap and Lake[33] offer an analytical alternative for calculating the full effective block permeability tensor.

Although the issue of heterogeneity, its upscaling, and its integration into predictive models has received considerable attention, detailed physical data for challenging our understanding is limited. To meet this need, a minipermeameter test system capable of acquiring spatially exhaustive suites of permeability data at each of a series of different sample supports was adapted.[34] Here, this technique is employed to physically characterize a cross-stratified block of Massillon sandstone exhibiting two nested-scales of heterogeneity: a small-scale feature defined by ubiquitous low-angle cross stratification and a large-scale feature defined by the bounding surfaces delineating the individual cross-stratified sets. Using a portion of the over 75,000 permeability measurements the interrelationship between heterogeneity, permeability patterns, and permeability upscaling is investigated. With these data answers to the following questions are explored: is there a relationship between the measured permeability characteristics and the visual aspects of the sampled block face; does the permeability upscale in a consistent and quantifiable manner; do the different scales of heterogeneity exhibit different upscaling behavior; do the permeabilities measured in different cross-stratified sets exhibit similar statistical characteristics and upscaling behavior?

Methods and Materials

Here, we present a brief overview of the experimental technique and a description of the Massillon sandstone sample. Our approach, involving the collection of large suites of permeability data at each of five different sample supports, has two distinguishing aspects. First, the permeability data are collected on a densely sampled grid. The spatially exhaustive nature of the data is necessary to quantify the distributional and spatial permeability statistics with a high degree of confidence. Second, all measurements, regardless of the sample support, are: 1) subject to consistent boundary conditions and flow geometries; 2) non-destructive, thus allowing all data to be collected from the same physical sample; and, 3) precise, subject to small and consistent measurement error. Such consistency in measurement is necessary for direct comparison of permeability data collected with different sample supports. By way of these controls, the acquired data are uniquely qualified for

investigating the interrelationship between heterogeneity, permeability patterns, and permeability upscaling.

Multi-Support Permeameter (MSP). Data were acquired with a specially designed minipermeameter[35-37] test system, termed the Multi-Support Permeameter (MSP).[34] Permeability is measured by simply compressing a tip seal against a flat, fresh rock surface while injecting gas at a constant pressure. Using information on the seal geometry, gas flow rate, gas injection pressure, and barometric pressure, the permeability is calculated using a modified form of Darcy's Law.[37] This process is automated by coupling a minipermeameter with an x-y positioner and computer control system. The minipermeameter functions as the measurement device of the MSP and consists of four electronic mass-flow meters (0-50, 0-500, 0-2000, and 0-20,000 cm^3/min. at standard conditions), a pressure transducer (0-100 kPa gauge), a barometer, and a gas temperature sensor that are all connected to a regulated source of compressed nitrogen. Measurements are made according to a user specified sampling grid programmed into the x-y positioner. Along with locating the tip seal for sampling, the positioner also compresses the tip seal squarely against the rock surface with a consistent and constant force. The minipermeameter and x-y positioner are configured with a computer control system to govern the data acquisition process and provide unattended operation of the MSP. A full description and analysis of the MSP is given by Tidwell and Wilson.[34]

MSP Tip Seals and the Sample Support. Measurements are made at different sample supports subject to consistent boundary conditions and flow geometries by simply varying the radius of the tip seal. Tip seals specifically designed for this program consist of a rigid aluminum housing to which a molded silicone rubber ring is affixed. A series of such tip seals have been built with inner radii (r_i) of 0.15, 0.31, 0.63, 1.27, and 2.54 cm, and an outer radii measuring twice the inner. A consistent and known tip seal geometry under compressed conditions is critical to precise measurement. For this reason, each of the tip seals is equipped with an internal spring-driven guide

to maintain a constant inner seal diameter. For the 0.63-cm and smaller tip seals, which experience considerable deformation on compression, an immobile outer guide is also employed.

It is important to note that the ring-shaped tip seal imposes a strongly divergent flow geometry on the test medium. The resulting non-uniform flow field not only has important implications relative to the measured permeability upscaling[38-40] but also raises questions concerning what the MSP actually measures. To address this latter issue, we investigated the measurement characteristics of the MSP theoretically[41] and empirically.[42] Results, as given by the calculated spatial weighting functions, indicate that the sample support is approximately hemispherical (additional work is necessary for strongly anisotropic media) consistent with the symmetry of the tip seal. Heterogeneities located near the tip seal influence the measurement more than those located further away, consistent with the divergent flow field imposed by the MSP. Also, as the tip seal size increases the effective radius, r_{eff}, of measurement increases. Although additional work is needed to fully quantify the sample support associated with each tip seal, we and others[37] believe that the r_{eff} is roughly proportional to r_i, hence the sample volume increases by a factor of 8 for each doubling of r_i.

Massillon Sandstone Sample. Permeability data were acquired from a 0.94 by 0.96 by 1.01-m block of Massillon sandstone purchased from the Briar Hill Stone Company in Glenmont, Ohio. The Massillon sandstone, of Pennsylvanian age, outcrops through much of northeastern Ohio and is an important commercial source of architectural stone. Based on thin-section analysis, this sample can be classified as a moderately well sorted, medium-grained quartz sandstone. Diagenetic alterations affecting the sandstone have occurred as evidenced by the presence of hydrous iron oxide precipitates and quartz overgrowths.

The fabric of the sandstone sample is characterized by a series of sub-horizontal bounding surfaces spaced approximately 16-22 cm apart (Fig. 1A). The bounding surfaces are planar with locally undulatory interfaces. Between the bounding surfaces low-angle cross stratification is evident with individual laminae spaced approximately 0.5-2 cm apart. In each of the cross-stratified sets (delineated by the bounding surfaces) the laminae are unidirectionally oriented with an apparent dip varying from 10° to 22°. Tangential contacts between the cross stratification and bounding surfaces are common.

The composition, sorting, and structure of the formation suggest that the Massillon sandstone was deposited subaqueously under relatively energetic conditions. However, there is some uncertainty concerning the actual mode of deposition, with both fluvial[43] and tidal environments[44] having been suggested.

Data Acquisition. Over 75,000 permeability measurements were collected from the six block faces of the Massillon sandstone sample. On each block face measurements were made with the 0.15-, 0.31-, 0.63-, 1.27-, and 2.54-cm r_i tip seals using the same sampling grid. The grid consisted of 2500 measurement points organized on a square 50 by 50 lattice on 1.27-cm centers. To avoid boundary effects on the measurement, the 62.2 by 62.2-cm grid was centered on each block face providing a buffer of over 15-cm between the grid and edge of the block. Although all six block faces were sampled, the following analysis is focused on data from a single block face cut normal to the cross stratification (we term Face 4), as data from the other five block faces exhibit similar statistical and upscaling characteristics.

It should be noted that each face of the Massillon sandstone block is marked by a small number of narrow voids. These voids appear to be the mold of some feature that subsequently weathered from the rock. MSP measurements made directly on or very near these voids have no real meaning because unrestrained gas flow occurred. As the voids are few and disconnected, the measured,

meaningless, permeability values were replaced with values representative of those near the feature. The missing values were replaced via ordinary kriging[45] using the retained permeability data (i.e., values measured away from the voids) and corresponding semivariograms (see below). A total of 15, 14, 14, 39, and 86 permeability values were replaced for the 0.15-, 0.31-, 0.63-, 1.27- and 2.54-cm tip seals, respectively. Thus, only 168 out of 12,500 measurements required replacement for this block face. Differences between summary statistics calculated with and without the replaced permeability values are almost indistinguishable. The adjustments are reflected in the data presented below.

Results

Here, we explore the permeability statistics and permeability upscaling measured on the Massillon sandstone sample. The analysis begins with the measured permeability fields and then progresses to the cumulative distribution function and semivariogram, respectively. Each statistical measure is analyzed with respect to its relation to the structural features visibly evident in the sampled block face and the manner with which it upscales. By upscaling, we mean the change in the statistic as the sample support (i.e., sample volume) increases. In each case analyses are performed for the entire block face and individually for each cross-stratified set. Although this analysis could encompass many statistical measures, the discussion is limited to select statistics, which were chosen so as to provide a reasonably broad basis of investigation. The selected statistics also form the basis for most geologic simulators and theoretical upscaling models.

Raw Permeability Data. The natural-log permeability fields ($\ln[k(y,z)]$ where k is in m^2, y is oriented parallel to the bounding surfaces, and z normal) measured with the 0.15-, 0.31-, 0.63-, 1.27- and 2.54-cm r_i tip seals are given in Figs. 1B-1F. Comparison of the permeability fields and photograph (Fig. 1A) reveal a remarkable similarity between the structural features visible in the rock face and the spatial patterns characterizing the two-dimensional permeability fields. Four well-defined sets of cross stratification, which we designate as Sets I-IV (see Fig. 1C), are delineated by

three bounding surfaces. These bounding surfaces are marked by zones of distinctly lower permeability that vary from 3-6 cm in thickness and fully span the width of the sampling domain. Between these bounding surfaces permeabilities are clearly higher and structured, exhibiting bands of alternating permeability, corresponding to the low-angle cross stratification.

Comparison of the permeability fields reveals upscaling, as evidenced by the distinct smoothing that accompanies increasing tip seal size. This smoothing reflects the preferential filtering of the small-scale structure associated with the low-angle cross stratification. That is, as the measurement becomes large compared to the small-scale feature, its signature becomes increasingly blurred. As the small-scale structure is filtered, the large-scale features associated with the three bounding surfaces become more apparent.

The sequential filtering of the small-scale heterogeneity is particularly evident in permeability transects extracted from the two-dimensional fields. Permeability (natural-log) transects oriented parallel (centered on $z = 20.3$ cm, see Fig. 1F) and normal to the bounding surfaces (centered on $y = 50.8$ cm) are plotted in Fig. 2. To facilitate comparison the log permeabilities for each tip seal have been normalized according to the mean log permeability of the transect. In both orientations the 0.15-cm tip seal transect is characterized by a relatively smooth large-scale structure on which a smaller-scale (high-frequency) feature is superimposed. As the tip seal size is increased the small-scale feature is sequentially filtered while the large-scale structure is preserved.

The small- and large-scale structures evident in these transects can be easily related to the cross-stratified features visible in the sampled block face. Normal to the bounding surfaces (Fig. 2B) a large-scale component, with a period of approximately 18-cm, and small-scale feature, with a period of approximately 3-cm, is evident. The large-scale feature exhibits three distinct cycles, each corresponding to a set of cross stratification (the fourth cycle is partially truncated as the bounding surface was excluded by the sampling grid). The associated small-scale structure is ubiquitous and

appears to be a product of the low-angle cross stratification comprising each set. Parallel to the bounding surfaces (Fig. 2A) both small- and large-scale structures are evident. Again, the small-scale structure appears related to permeability variations arising from the low-angle cross stratification, while the large-scale structure (with a period of approximately 50 cm) is believed to be the result of changes in the sediment source coincident with the progradation of the bedform.

Cumulative Distribution Functions. The cumulative distribution functions (CDFs) for the natural-log permeability data measured with the five different-size tip seals are given in Fig. 3. Each of the CDFs is characterized by a distinct negative skew, which suggests the permeability is not log-normally distributed. The skewness is largely a product of the bands of lower permeability associated with the bounding surfaces, particularly Set IV. Even with this skewness, the total range in permeability spanned by the five CDFs is relatively narrow, approximately six natural log cycles or just over two orders of magnitude on an arithmetic scale.

Several changes in the CDFs are evident with increasing tip seal size. Subtle differences are noted across the entire distribution; however, the most significant changes occur in the lower tail. As the tip seal size increases there is a decrease in the skew. Rather than the distribution becoming symmetric, a bimodal structure appears. The two modes are distinguishable in the CDFs for 1.27- and 2.54-cm tip seals by the offset evident between the 1st to 5th percentiles. This trend toward a weak bimodal distribution reflects the organization of the permeability field into alternating bands of "high-" and "low-permeability" (see Fig. 1); that is, the small-scale variability is filtered from the permeability field leaving a simple layered system (i.e., the large-scale structure). Also, the mean and variance of the CDFs change with increasing sample support. To explore this behavior in more detail, the mean and variance of the natural-log permeability are plotted as a function of the inner tip seal radius in Fig. 4 ("all sets"). Both upscale according to power-law relation (see below) in which the mean increases with increasing sample support (i.e., sample volume), while the variance decreases. Although not shown, these trends extend to larger scales. A single permeability

measurement that integrates over much of the sampling domain was made with a large tip seal (7.62-cm r_i) centered on the sampling grid. Its measured value, -26.2 m^2, is consistent with the trend shown in Fig. 4A. Likewise, the variance is seen to asymptotically approach a value of zero, which must be achieved when the characteristic length of measurement equals the dimension of the sampling grid.

CDFs were also calculated for individual sets of cross stratification. Results for Sets II and IV are given in Fig. 5. In general, there are relatively few differences between these CDFs, which consistently exhibit an upper log permeability (m^2) range between -26.4 and -25.8, a negative skew that decreases with increasing sample support, and an increasing mean and decreasing variance with increasing tip seal size. Where the CDFs tend to differ is in the minimum range of the distribution and in the detailed shape of the distribution. The noted similarities in the CDFs occur because the same depositonal process formed each cross-stratified set, while differences reflect variations in flow velocity, flow direction, and/or sediment load between the events responsible for depositing each particular cross-stratified set.

The mean and variance upscaling for individual cross-stratified sets are compared to each other and to that for the entire block face (all sets) in Fig. 4. To aid in this comparison, a power-law function has been fitted to each plot

$$Y_i = c(r_i)^{\alpha}, \qquad (1)$$

where Y_i is the mean or variance of the natural-log permeability, c is a proportionality factor, α is the power-law exponent, and the subscript i designates tip seal size. The means for each of the cross stratified sets and the entire block face follow very similar upscaling trends. This is evidenced by the fact that we were able to fit a power law function using the same exponent, $\alpha = -0.015$, to each

of the five curves. The same is true of the variance upscaling where an exponent of $\alpha = -0.35$ was used. Where the cross-stratified sets differ is in the magnitude of their means and variances. The c values fitted to the mean upscaling curves differ by a factor of 1.02, while the fitted c values for the variance differ by a factor of 6. These offsets may be slightly overestimated as the bounding surface for Set I, which exhibits a high mean and low variance relative to the others, was truncated from the analysis by the position of the sampling grid.

Spatial Structure. The spatial correlation of the natural-log permeability data was also investigated. Full two-dimensional semivariograms were calculated for each of the five tip seals using Fourier analysis (via the Fast Fourier Transform).[42,46] The two-dimensional semivariogram for the 0.15 cm tip seal is given in Fig. 6 for reference. In addition, transects oriented parallel and normal to the bounding surfaces, and taken through the center of the two-dimensional semivariograms, are plotted in Fig. 7. To quantify the spatial structure, semivariogram models were fit to each of the transects (Fig. 7). Two nested anisotropic exponential models coupled with a cosine hole-effect model (applied only in the z direction, normal to the bounding surfaces) closely fit the sample semivariograms. The composite fitted model γ is given by

$$\gamma(\vec{s}) = \sigma_1^2\left(1-\exp\left[-\frac{3\vec{s}}{\vec{\lambda}_1}\right]\right)+\sigma_2^2\left(1-\exp\left[-\frac{3\vec{s}}{\vec{\lambda}_2}\right]\right)+\sigma_3^2\left(1-\cos\left[\frac{2\pi s_z}{T_z}\right]\right), \quad \text{.....(2)}$$

where σ_j^2 is the variance component for the jth model $(j = 1,2,3)$, $\vec{\lambda}_j$ is the semivariogram range (cm) in the principal directions $\left(\vec{\lambda} = \left(\lambda_y, \lambda_z\right)\right)$ for the jth model, T_z (cm) is the period of the hole-effect feature, and $\vec{s} = \left(s_y, s_z\right)$ is the separation vector (cm) in the principal directions. The fitted models are given in Fig. 7 by the solid lines while the corresponding parameters are presented in Table 1.

The characteristics of the semivariograms are easily related to the structural features visible in the sampled block face (Fig. 1A). The semivariograms reveal a strong degree of anisotropy reflecting the stratified structure of the Massillon sandstone sample. Long-range spatial correlation is apparent parallel to the bounding surfaces while shorter-range correlation, with a strong hole-effect, is exhibited normal to the bounding surfaces (Fig. 7). The distinct hole-effect reflects the presence of multiple cross-stratified sets, each of relatively similar thickness and permeability characteristics. The semivariogram transects also indicate the presence of two nested structural features, a large-scale feature associated with the cross-stratified sets and a small-scale feature defined by the low-angle cross stratification within each set.

The fitted range values agree closely with the length scales inferred from visual inspection of the sampled block face. The large-scale feature with horizontal range exceeding the length of the semivariogram is consistent with the laterally continuous nature of the cross-stratified sets, while the period with which the vertically oriented semivariogram transect oscillates is consistent with the distance between sets. The small-scale feature shows only slight anisotropy and is defined by a range equal to the average spacing between lamina of the intraset cross stratification.

Several upscaling trends are evident among the calculated semivariograms. First, the sill of the semivariogram decreases with increasing sample support, reflecting the accompanying decrease in variance. Second, the fitted semivariogram range values appear to increase with increasing tip seal size (see Table 1). The range upscaling simply reflects the fact that as the tip seal size increases, two measurements must be separated that much further apart (i.e., proportional to the increasing r_{eff}) before they become completely uncorreltated.[47,48] Although a number of trends are noted among the fitted parameters, the general semivariogram model (Eq. 2) remains essentially unaffected by changing sample support. Exceptions are the semivariograms for the 1.27- and 2.54-cm tip seals, which fail to resolve the small-scale structure associated with the low-angle cross stratification. This

occurs because the size of the tip seal has become large with respect to the low angle cross-stratification, thus filtering its signature from the permeability field.

The variance upscaling associated with each of the structural features identified in the semivariograms is also explored. The variances corresponding to the small-scale feature, the large-scale feature, and the hole-effect feature were determined from the fitted semivariogram model parameters in Table 1 (σ_1^2, σ_2^2, and σ_3^2 in Eq. 2, respectively). These variances are plotted as a function of the inner tip seal radius in Fig. 8. In each case the variances follow smooth but different upscaling trends. The greatest loss of variance is associated with the small-scale feature. The variance for the large-scale feature exhibits a gradual decline that accelerates with increasing tip seal size. The variance associated with the hole-effect structure exhibits relatively minor variation over all tip seal sizes. These plots demonstrate that the heterogeneities associated with structures smaller than the tip seals, or more specifically r_{eff}, are filtered from the data, while the heterogeneities associated with structures larger than the tip seals are preserved in the data.

Two-dimensional semivariograms were also calculated for each of the individual cross-stratified sets. Semivariograms for the 1.27-cm tip seal are plotted in Fig. 9 for Sets II and IV. Both cross-stratified sets exhibit distinct anisotropy with the principal axes oriented at an inclined angle to the horizontal. Although not shown, both sets also exhibit similar upscaling trends, characterized by a decreasing semivariogram sill, increasing range, and a consistent semivariogram structure with increasing tip seal size. A notable difference between the two cross-stratified sets is the orientation of the principal permeability axes, and hence the orientation of the cross stratification. In Set II the cross stratification is inclined at an angle of 10° while Set IV it is inclined at an angle of 22°, consistent with the orientation of the cross stratification visibly evident in the sampled block face (Fig. 1A). This difference is likely the result of changes in the sediment load and/or flow conditions between depositional events.

Discussion

Here, we explore implications of the heterogeneity, permeability patterns, and permeability upscaling measured on the Massillon sandstone sample. Three different results are discussed, each with bearing on the characterization and modeling of heterogeneous geologic materials.

First, distinct similarities were identified between the spatial characteristics of the permeability data and the visual attributes of the sampled block face. This result provides encouraging evidence that the textural and structural patterns visibly evident in a rock sample can be used to characterize the spatial patterns and spatial statistics of its permeability. Establishing such a relationship is particularly important in the context of reservoir characterization where permeability data are generally a limited commodity. Currently, we are quantitatively investigating this relation by comparing these permeability fields and others with digitized photographic images of the corresponding block faces, while we assess the textural and diagenetic controls on the measured permeability through detailed analysis of thin-sections taken from the Massillon sandstone sample.

Second, summary statistics calculated for the individual cross-stratified sets were found to exhibit the same general characteristics as that of the integrated sample taken across all sets. This similarity is believed to result from a general consistency in the depositional processes forming the individual cross-stratified sets. It also suggests that many of the important statistical characteristics of permeability can be reconstructed directly from the summary information contained in the integrated sample statistics. However, some potentially important features are not resolved, including the difference in the mean/variance between cross-stratified sets and the orientation of the low-angle cross stratification.

Third, the upscaling trends exhibited by the permeability statistics are qualitatively consistent with the basic concepts of volume averaging. Specifically, measurements made with larger tip seals

(i.e., sample supports) integrate over more heterogeneity, with those features smaller than the tip seal being preferentially filtered from the data. This is evident in the permeability fields (Fig. 1), transects (Fig. 2), and semivariograms (Fig. 7) where the small-scale structure associated with the low-angle cross stratification is sequentially filtered from the data, while the signature of the large-scale bounding surfaces is preserved. Larger tip seals sequentially integrating over more heterogeneity also explain the decreasing variance (Fig. 4B) and decreasing semivariogram sill (Fig. 7). The increasing semivariogram range is explained by the increasing r_{eff} accompanying the increasing tip seal radius (Table 1).

However, inspection of the mean upscaling suggests that the spatial averaging process may not be so simple. The fact that the mean of the natural-log permeability (Fig. 4A) increases with increasing sample support leads us to conclude that the Massillon sandstone sample does not upscale according to a geometric averaging process. We also note that the sample does not upscale according to an arithmetic averaging process, as the arithmetically averaged mean also increases with scale ($E[k_i(\vec{x})] = 1.14$, 1.43, 1.86, 2.50, 3.42, and 4.18 x10^{-12} m^2 for the 0.15- to 7.62-cm r_i tip seals). Considering the spatially exhaustive nature of the permeability data, this result indicates that something beyond the heterogeneous characteristics of the medium is contributing to the measured upscaling. We believe that this other factor involves the non-uniform flow conditions imparted by the minipermeameter measurements. The measured upscaling is the result of five distinct scales of measurement (i.e., none of our measurements are made with a support of negligible volume, that is a point-support), each employing non-uniform flow conditions, and each interacting with an anisotropic medium possessing nested scales of heterogeneity. As a full discussion of this effect is beyond the scope of the present paper, we refer the interested reader to other papers[49,50] where a more thorough review is given.

Conclusions

A comprehensive suite of data characterizing the spatial permeability patterns and permeability upscaling for a cross-bedded sandstone exhibiting nested scales of heterogeneity was presented. Analyses were based on over 75,000 permeability measurements (with over 12,000 shown here) collected from a meter-scale block of Massillon sandstone. These studies were made possible through the use of a novel experimental system, termed the Multi-Support Permeameter (MSP). With this system suites of spatially exhaustive permeability data were collected at five different sample supports (i.e., sample volumes), each subject to the same measurement conditions. Here, the results are summarized in the context of the questions raised in the introduction to this paper.

1. The spatial statistics of the permeability are related to the structural attributes of the sandstone sample. Evidence supporting this relationship include, the visual similarity between the permeability patterns and the structural characteristics of the sandstone; and, the consistency between the characteristics of the calculated semivariograms (length scales, anisotropy ratios, orientation of principal permeability axes) and the physical size, shape, and orientation of the features visibly discernable in the sampled rock face.

2. The permeability statistics exhibit distinct and consistent trends with increasing sample support (i.e., upscaling); specifically, the two-dimensional permeability fields become smoother; the CDFs are characterized by an increasingly bimodal shape; the variance decreases and the mean increases according to a power-law relation; the semivariogram range increases; while the general structure of the semivariogram (anisotropic, exponential model with coupled hole-effect) remains essentially unchanged.

3. Different scales of heterogeneity upscale differently. As the size of the tip seal becomes increasingly large relative to the low-angle cross stratification, this small-scale structure is

preferentially filtered from the permeability distribution, while the large-scale structure is preserved. This filtering effect is evident in the permeability fields, transects, CDFs, and the semivariograms.

4. Individual cross-stratified sets exhibit similar statistical and upscaling characteristics suggesting that consistency in depositional process results in relatively consistent statistical characteristics and upscaling behavior. However, some differences do exist between sets (e.g., mean permeability, permeability variance, and orientation of the low-angle cross stratification), which likely reflect changes in the flow velocity, flow orientation, sediment load, and/or size distribution of the sediment between depositional events.

Nomenclature

c = power-law proportionality factor, units depend on Y and α

i = subscript denoting tip seal size

j = subscript denoting nested semivariogram model

k = permeability, L^2, m^2

r_{eff} = effective radius of minipermeameter measurement, L, cm

r = inner tip seal radius, L, cm

$\vec{s}$ = separation vector in the principal directions (s_y, s_z), L, cm

T = period of cosine hole-effect structure, L, cm

Y = natural-log permeability summary statistic

y = spatial coordinate oriented parallel to the bounding surfaces, L, cm

z = spatial coordinate oriented normal to the bounding surfaces, L, cm

α = power-law exponent

γ = semivariogram of the natural-log permeability

$\vec{\lambda}$ = semivariogram range in the principal directions (λ_y, λ_z), L, cm

σ^2 = variance of the natural-log permeability

Acknowledgments

The authors wish to thank Mark Bailey for his help in data collection and Allan Gutjahr, Robert Glass, Peter Mozley, and Fred Phillips for providing constructive advice throughout this effort. We also extend our gratitude to Mike Chapin, Peter Davies, Robert Holt, and two anonymous reviewers whose comments significantly contributed to this paper. This work was supported by the U.S. Department of Energy, Office of Basic Energy Science, Geoscience Research Program, under contracts DE-AC04-94AL85000 and DE-F303-96ER14589/A000. Sandia is a multiprogram laboratory operated by Sandia Corporation, a Lockheed Martin Company, for the United States Department of Energy.

References

1. Journel, A.G.: "Constrained Interpolation and Qualitative Information-The Soft Kriging Approach," *Mathematical Geology* (1986) 18, 269-286.

2. Gelhar, L.W.: "Stochastic Subsurface Hydrology from Theory to Applications," *Water Resources Research* (1986) 22, No. 9, 135S-145S.

3. Davis, J.M. et al.: "Architecture of the Sierra Ladrones Formation, Central New Mexico: Depositional Controls on the Permeability Correlation Structure," *Geol. Soc. Am. Bull.* (1993) 105, No. 8, 998-1007.

4. Jordan, D.W. and Pryor, W.A.: "Hierarchical Levels of Heterogeneity in a Mississippi River Meander Belt and Application to Reservoir Systems," *AAPG Bull.* (1992) 76, No. 10, 1601-1624.

5. Istok, J.D. et al.: "Spatial Variability in Hydrologic Properties of a Volcanic Tuff," *Groundwater* (1994) 32, No. 5, 751-760.

6. Phillips, F.M. and Wilson, J.L.: "An Approach to Estimating Hydraulic Conductivity Spatial Correlation Scales Using Geological Characteristics," *Water Resources Research* (1989) 25, No. 1, 141-143.

7. Journel, A.G. and Alabert, F.: "Non-Gaussian Data Expansion in the Earth Sciences," *Terra Nova* (1989) 1, 123-129.

8. Dagan, G.: "Statistical Theory of Groundwater Flow and Transport : Pore to Laboratory, Laboratory to Formation, and Formation to Regional Scale," *Water Resources Research* (1986) 22, No. 9, 120S-134S.

9. Haldorsen, H.H.: "Simulator Parameter Assignment and the Problem of Scale in Reservoir Engineering," *Reservoir Characterization*, L.W. Lake and H.B. Carroll Jr.(eds.), Academic Press, San Diego (1986) 293-340.

10. Warren, J.E. and Price, H.S.: "Flow in Heterogeneous Porous Media," *SPEJ* (1961) 153-169.

11. Kirkpatrick, S.: "Percolation and Conduction," *Reviews of Modern Physics* (1973) 45, No. 4, 574-588.

12. Gutjahr, A.L. et al.: "Stochastic Analysis of Spatial Variability in Subsurface Flows, 2, Evaluation and Application," *Water Resources Research* (1978) 14, No. 5, 953-960.

13. Deutsch, C.V.: "Calculating Effective Absolute Permeability in Sandstone/Shale Sequences," *SPEFE* (March 1989) 343-348.

14. King, P.R.: "The Use of Renormalization for Calculating Effective Permeability," *Transport in Porous Media* (1989) 4, No. 1, 37-58.

15. Rajaram, H. and McLaughlin, D.: "Identification of Large-Scale Spatial Trends in Hydrologic Data," *Water Resources Research* (1990) 26, No. 10, 2411-2423.

16. Rubin, Y.: "Flow and Transport in Bimodal Heterogeneous Formations," *Water Resources Research* (1995) 31, No. 10, 2461-2468.

17. Hewett, T.A.: "Fractal Distributions of Reservoir Heterogeneity and Their Influence on Fluid Transport," paper SPE 15386 presented at the 1986 Annual Technical Conference and Exhibition, New Orleans, 5-8 October.

18. Neuman, S. P.: "Generalized Scaling of Permeabilities: Validation and Effect of Support Scale," *Geophysical Review Letters* (1994) 21, No. 5, 349-353.

19. Di Federico, V. and Neuman, S.P.: "Scaling of Random Fields by Means of Truncated Power Variograms and Associated Spectra," *Water Resources Research* (1997) 33, No. 5, 1075-1085.

20. Liu, H.H. and Molz, F.J.: "Multifractal Analyses of Hydraulic Conductivity Distributions," *Water Resources Research* (1997) 33, No. 11, 2483-2488.

21. Cushman, J.H.: "An Introduction to Hierarchical Porous Media," *Dynamics of Fluids in Hierarchical Porous Media*, J.H. Cushman (ed.), Academic Press, New York (1990) 1-6.

22. Goggin, D.J. et al.: "Patterns of Permeability in Eolian Deposits: Page Sandstone (Jurassic), Northeastern Arizona," *SPEFE*, (March 1986) 297-306.

23. Chandler, M.A. et al.: "Effects of Stratigraphic Heterogeneity on Permeability in Eolian Sandstone Sequence, Page Sandstone, Northern Arizona," *AAPG Bull.* (1989) 73, No. 5, 658-668.

24. Corbett, P.W.M. and Jensen, J.L.: "Application of Probe Permeametry to the Prediction of Two-Phase Flow Performance in Laminated Sandstones (lower Bent Group, North Sea)," *Marine and Petroleum Geology* (1993) 10, 335-346.

25. Robertson, R.W. and Caudle, B.H.: "Permeability Continuity of Laminae in the Calvin Sandstone," *JPT* (1971) 661-670.

26. Kortekaas, T.F.M.: "Water-Oil Displacement Characteristics in Cross-Bedded Reservoir Zones," *SPEJ* (1985) 917-926.

27. Van De Graaff, W.J.E. and Ealey, P.J.: "Geological Modeling for Simulation Studies," *AAPG Bull.* (1989) 73, No. 11, 1436-1444.

28. Ringrose, P.S. et al.: "Relevant Reservoir Characterization: Recovery Process, Geometry, and Scale," *In Situ* (1993) 17, No. 1, 55-82.

29. Bierkens, M.F.P. and Weerts, H.J.T.: "Block Hydraulic Conductivity of Cross-Bedded Fluvial Sediments," *Water Resources Research* (1994) 30, No. 10, 2665-2678.

30. Kyte, J.R. and Berry, D.W.: "New Pseudofunctions to Control Numerical Dispersion," *SPEJ* (1975) 269-276.

31. Lasseter, T.J., Waggoner, J.R. and Lake, L.W.: "Reservoir Heterogeneities and Their Influence on Ultimate Recovery," *Reservoir Characterization*, L.W. Lake and H.B. Carroll Jr. (eds.), Academic Press, New York (1986) 545-560.

32. Kossack, C.A., Aasen, J.O. and Opdal, S.T.: "Scaling Up Heterogeneities with Pseudofunctions," *SPEFE* (March 1990) 226-232.

33. Kasap, E. and Lake, L.W.: "Calculating the Effective Permeability Tensor of a Gridblock," *SPEFE* (February 1990) 192-200.

34. Tidwell, V.C. and Wilson, J.L.: "Laboratory Method for Investigating Permeability Upscaling," *Water Resources Research* (1997) 33, No. 7, 1607-1616.

35. Dykstra, H. and Parsons, R.L.: "The Prediction of Oil Recovery by Water Flood," *Secondary Recovery of Oil in the United States, 2nd ed.*, API, New York (1950) 160-174.

36. Eijpe, R. and Weber, K.J.: "Mini-Permeameters for Consolidated Rock and Unconsolidated Sand," *AAPG Bull.* (1971) 55, No. 2, 307-309.

37. Goggin, D. J., Thrasher, R. L. and Lake, L. W.: "A Theoretical and Experimental Analysis of Minipermeameter Response Including Gas Slippage and High Velocity Flow Effects," *In Situ* (1988) 12, No. 1-2, 79-116.

38. Matheron, G.: "*Elements Pour une Theorie des Milieux Poreux*," Maisson et Cie, Paris (1967).

39. Desbarats, A.J.: "Spatial Averaging of Transmissivity in Heterogeneous Fields with Flow Toward a Well," *Water Resources Research* (1992) 28, No. 3, 757-767.

40. Indelman, P. and Abramovich, B.: "Nonlocal Properties of Nonuniform Averaged Flows in Heterogeneous Media," *Water Resources Research* (1994) 30, No. 12, 3385-3393.

41. Aronson, E. and Wilson, J.L.: "Calculating Instrument Spatial Filter Functions: Illustrated for the Gas Minipermeameter," Abst, *EOS* 80(46), F440, 1999 Fall Meeting of the AGU, San Francisco, December 13-17.

42. Tidwell, V.C., Gutjahr, A.L. and Wilson, J.L.: "What Does an Instrument Measure? Empirical Spatial Weighting Functions Calculated from Permeability Data Sets Measured on Multiple Sample Supports," *Water Resources Research* (1999) 35, No. 1, 43-54.

43. Schmidley, E.B.: "*The Sedimentology, Paleogeography and Tectonic Setting of the Pennsylvanian Massillon Sandstone in East-Central Ohio*," MS Thesis, U. Akron, Akron (1987).

44. Gray, H.H.: "Petrology of the Massillon Sandstone at the Type Locality," *The Ohio Journal of Science* (1956) 56, No. 3, 138-146.

45. Deutsch, C.V. and Journel, A.G.: "*GSLIB: Geostatistical Software Library and User's Guide*," Oxford University Press, New York (1997).

46. Bracewell, R.N.: "*The Fourier Transform and Its Applications*," McGraw-Hill Book Co. Inc., New York (1986).

45. Deutsch, C.V. and Journel, A.G.: "*GSLIB: Geostatistical Software Library and User's Guide*," Oxford University Press, New York (1997).

46. Bracewell, R.N.: "*The Fourier Transform and Its Applications*," McGraw-Hill Book Co. Inc., New York (1986).

47. Clark, I.: "Regularization of a Semi-Variogram," *Computers and Geosciences* (1977) 3, 341-346.

48. Journel, A G. and Huijbregts, C.J.: "*Mining Geostatistics*," Academic Press, New York (1978).

49. Tidwell, V.C. and Wilson, J.L.: "Permeability Upscaling Measured on a Block of Berea Sandstone: Results and Interpretation," *Mathematical Geology* (1999) 31, No. 7, 749-769.

50. Tidwell, V.C. and Wilson, J.L.: "Upscaling Experiments Conducted on a Block of Volcanic Tuff: Results for a Bimodal Permeability Distribution," *Water Resources Research* (1999) 35, No. 11, 3375-3387.

SI Metric Conversion Factors

in. x 2.54* E+00 = cm

ft^2 x 9.290304* E-02 = m^2

*Conversion factor is exact.

Table 1. Parameter values for the semivariogram models (Eq. 2) fitted to the data given in Fig. 7.

Tip Seal	Small-Scale Structure			Large-Scale Structure			Hole-Effect Structure	
	σ_1^2	$\lambda_{y,1}$ (cm)	$\lambda_{z,1}$ (cm)	σ_2^2	$\lambda_{y,2}$ (cm)	$\lambda_{z,2}$ (cm)	σ_3^2	T_z (cm)
0.15 cm	0.17	2.7	1.5	0.23	33.0	18	0.055	18.0
0.31 cm	0.06	3.3	2.1	0.23	34.8	19.5	0.065	18.0
0.63 cm	0.02	4.5	3.3	0.22	57.0	22.5	0.080	18.0
1.27 cm	-	-	-	0.20	63.0	28.5	0.090	18.0
2.54 cm	-	-	-	0.15	75.0	40.5	0.068	18.0

Figure Captions

Fig. 1-Photograph A) of Face 4 of the Massillon sandstone sample showing the area sampled with the MSP. The corresponding natural-log permeability fields (where k is in m^2) measured with the B) 0.15-, C) 0.31-, D) 0.63-, E) 1.27-, and F) 2.54-cm r_i tip seals are also given. Data were collected from a 50 by 50 point grid on 1.27-cm centers. Also shown are (C) the inferred bounds for each of the cross-stratified sets, and (F) locations for the permeability transects given in Fig. 2.

Fig. 2-Permeability (natural-log) transects measured with each of the five MSP tip seals. Shown are transects oriented A) parallel to stratification centered on z=20.3 cm (see Fig. 1F), and B) normal to stratification centered on y=50.8 cm. To facilitate comparison, each transect was normalized by its mean log permeability.

Fig. 3-Cumulative distribution functions for the natural-log permeability data given in Fig. 1. Each curve represents N=2500 permeability values.

Fig. 4-Mean (A) and variance (B) upscaling plotted versus the inner tip seal radius. Shown are the upscaling trends for each individual set of cross stratification and for the entire block face ("all sets"). In each case a power-law model (Eq. 1) is fit to the calculated statistic (symbols).

Fig. 5-Cumulative distribution functions for individual sets of cross stratification. Shown are the CDFs for A) Set II (N=650) and B) Set IV (N=650, see Fig. 1C).

Fig. 6-Two-dimensional semivariogram calculated from the natural-log permeability data collected with the 0.15 cm r_i tip seal.

Fig. 7-Semivariogram transects (symbols) for the natural-log permeability data measured with each of the five different-size tip seals. Orientation is A) parallel (y axis) and B) normal (z axis) to the bounding surfaces. The fitted semivariogram models (Eq. 2) are given by solid lines.

Fig. 8-Variance upscaling associated with each semivariogram structural feature (Eq. 2 and Table 1) plotted versus inner tip seal radius.

Fig. 9-Two-dimensional semivariograms calculated for individual sets of cross stratification. Shown are the 1.27-cm tip seal semivariograms for A) Set II, and B) Set IV.

About the Authors

Vincent C. Tidwell vctidwe@sandia.gov

Since 1990, Vincent C. Tidwell has been a research hydrologist at Sandia National Laboratories in Albuquerque, New Mexico. He received his B.S. degree in geology from the University of Texas at Arlington in 1985, his M.S. degree in hydrology from the University of Arizona in 1988, and his Ph.D. in hydrogeology from the New Mexico Institute of Mining and Technology in 1999. His research interests include physical investigation of spatial variability and upscaling processes, single/multiphase flow and transport in fractured rocks, and visualization/imaging technology.

John L. Wilson jwilson@nmt.edu

John L. Wilson is Professor of Hydrology and Chairman of the Department of Earth and Environmental Sciences at the New Mexico Institute of Mining and Technology in Socorro, New Mexico. He received his B.C.E. degree from the Georgia Institute of Technology in 1968, and his Ph.D. degree in Hydrodynamics from MIT in 1974. After teaching on the faculty at MIT for eight years he briefly joined INTERA Inc. in Houston, before taking a position as Director of the Hydrology Program at New Mexico Tech. His research interests include permeable media fluid flow and transport, using field & laboratory experiments and mathematical models to examine the movement of water, oil, dissolved chemicals, colloids, and bacteria through porous, fractured, and faulted media.

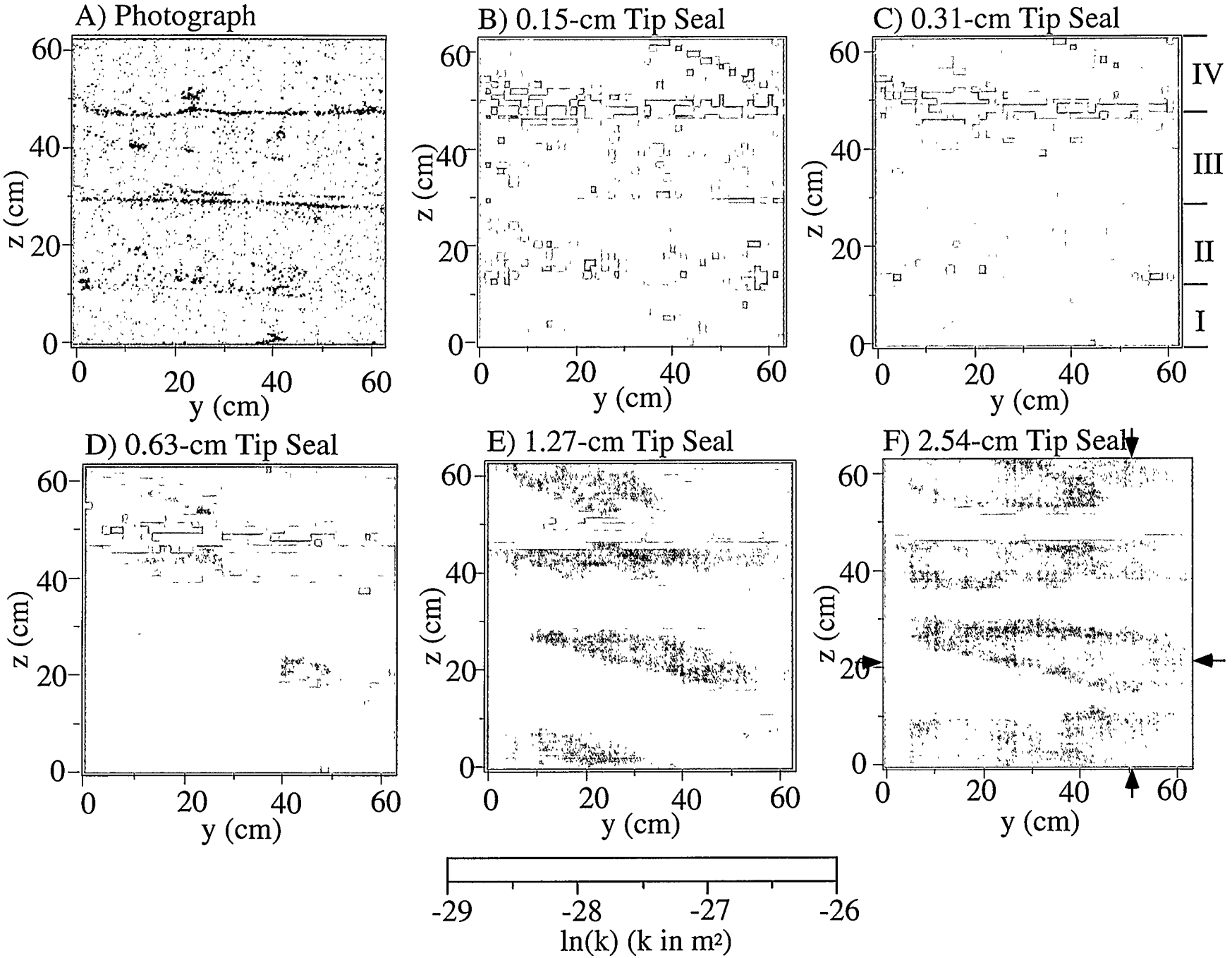
A) Photograph
B) 0.15-cm Tip Seal
C) 0.31-cm Tip Seal
D) 0.63-cm Tip Seal
E) 1.27-cm Tip Seal
F) 2.54-cm Tip Seal
z (cm)
y (cm)
0
20
40
60
IV
III
II
I
-29
-28
-27
-26
ln(k) (k in m²)

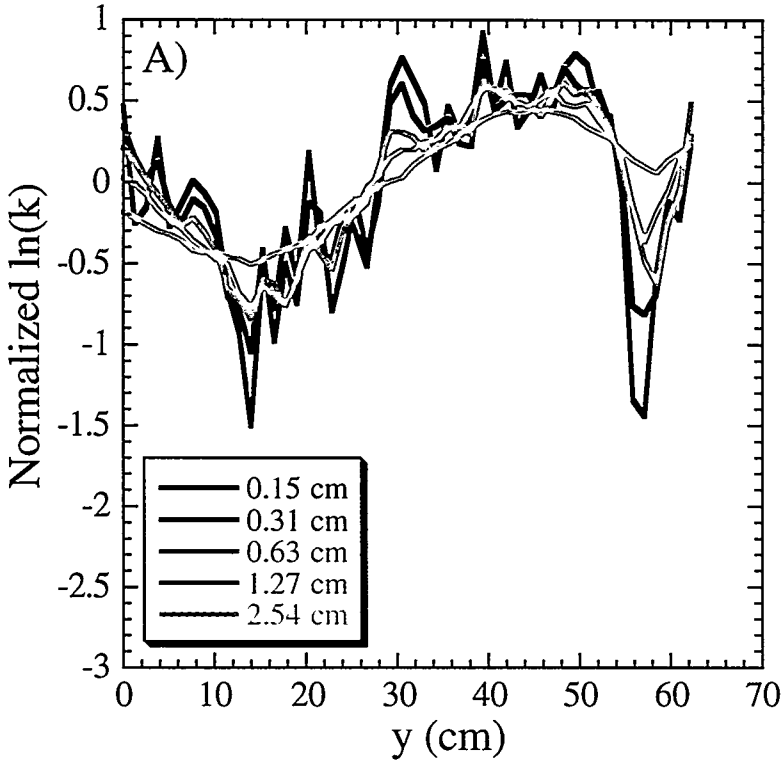
A)
Normalized ln(k)
y (cm)
0.15 cm
0.31 cm
0.63 cm
1.27 cm
2.54 cm

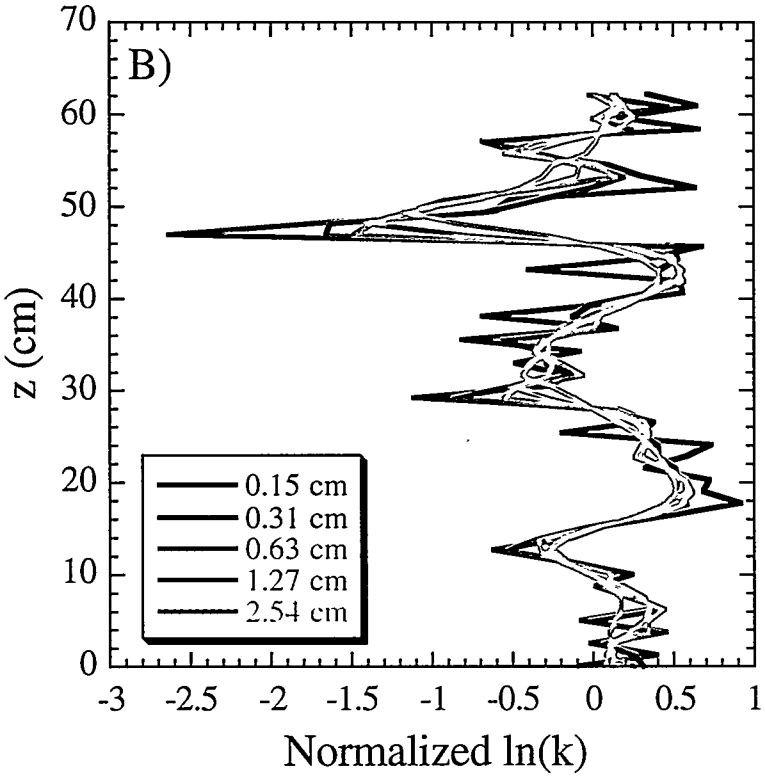
B)
z (cm)
Normalized ln(k)
0.15 cm
0.31 cm
0.63 cm
1.27 cm
2.54 cm

Fig 3

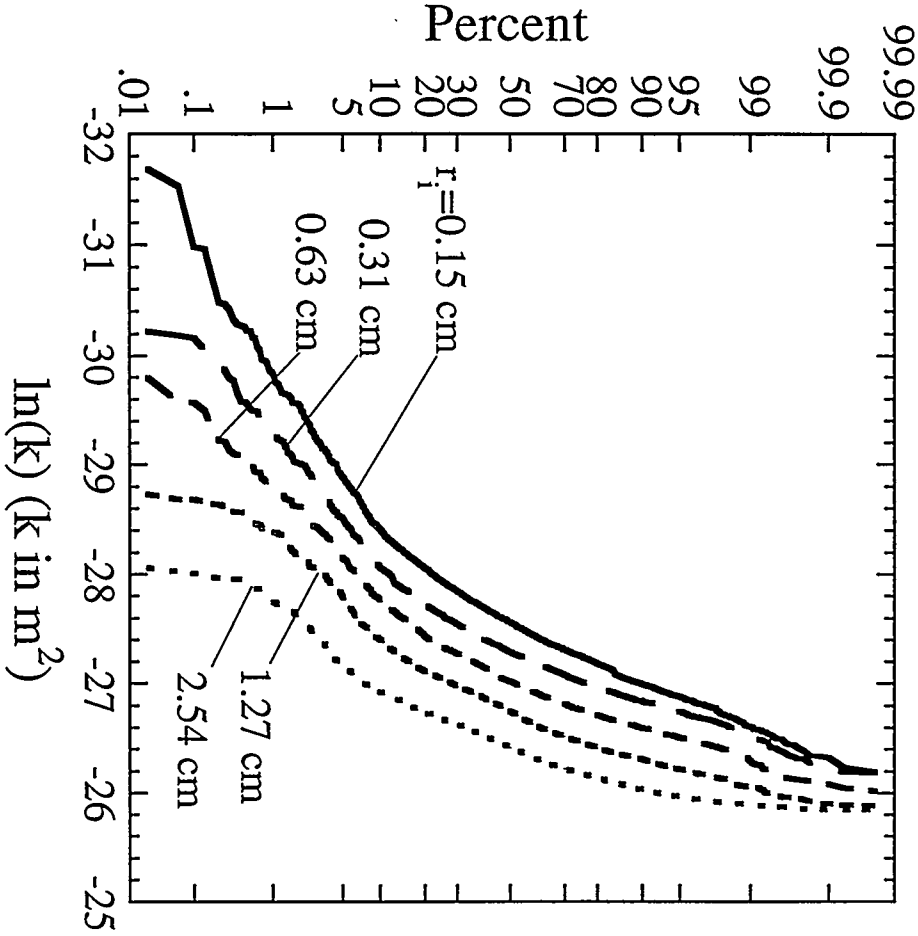
Percent
99.99
99.9
99
95
90
80
70
50
30
20
10
5
1
.1
.01
-32
-31
-30
-29
-28
-27
-26
-25
ln(k) (k in m²)
r_i=0.15 cm
0.31 cm
0.63 cm
1.27 cm
2.54 cm

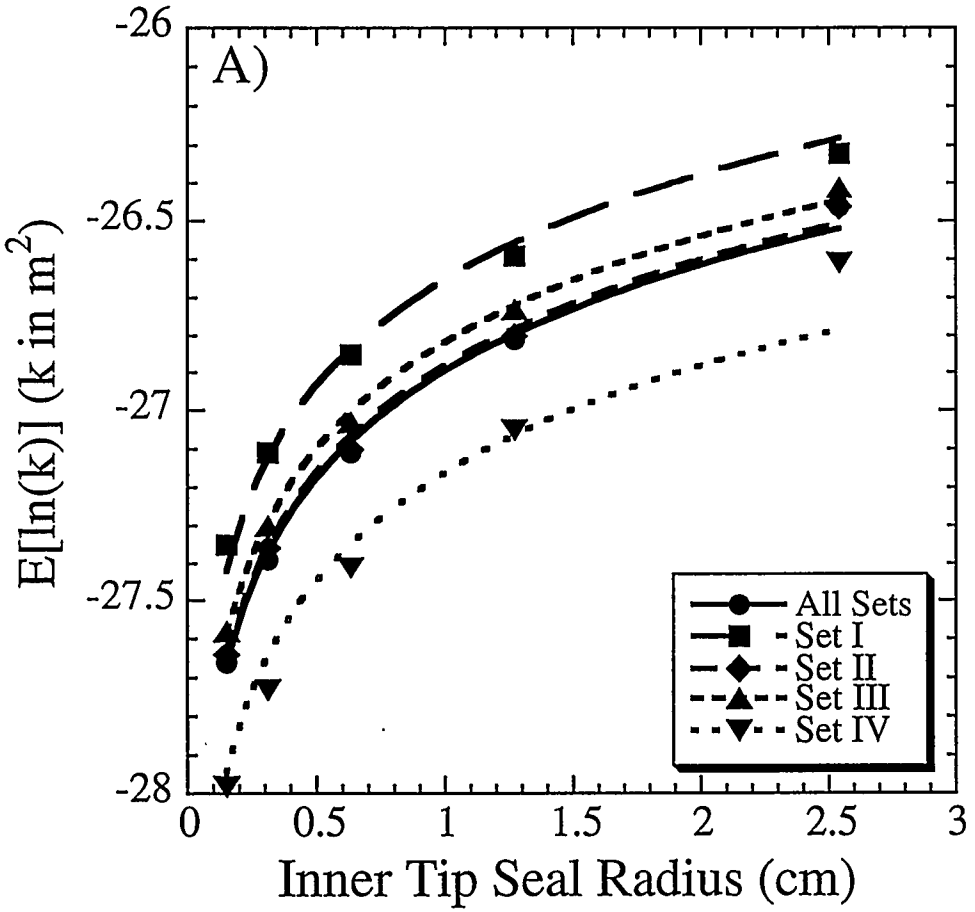
A)
-26
-26.5
-27
-27.5
-28
0
0.5
1
1.5
2
2.5
3
E[ln(k)] (k in m^2)
Inner Tip Seal Radius (cm)
All Sets
Set I
Set II
Set III
Set IV

Fig 4a

Fig 4B

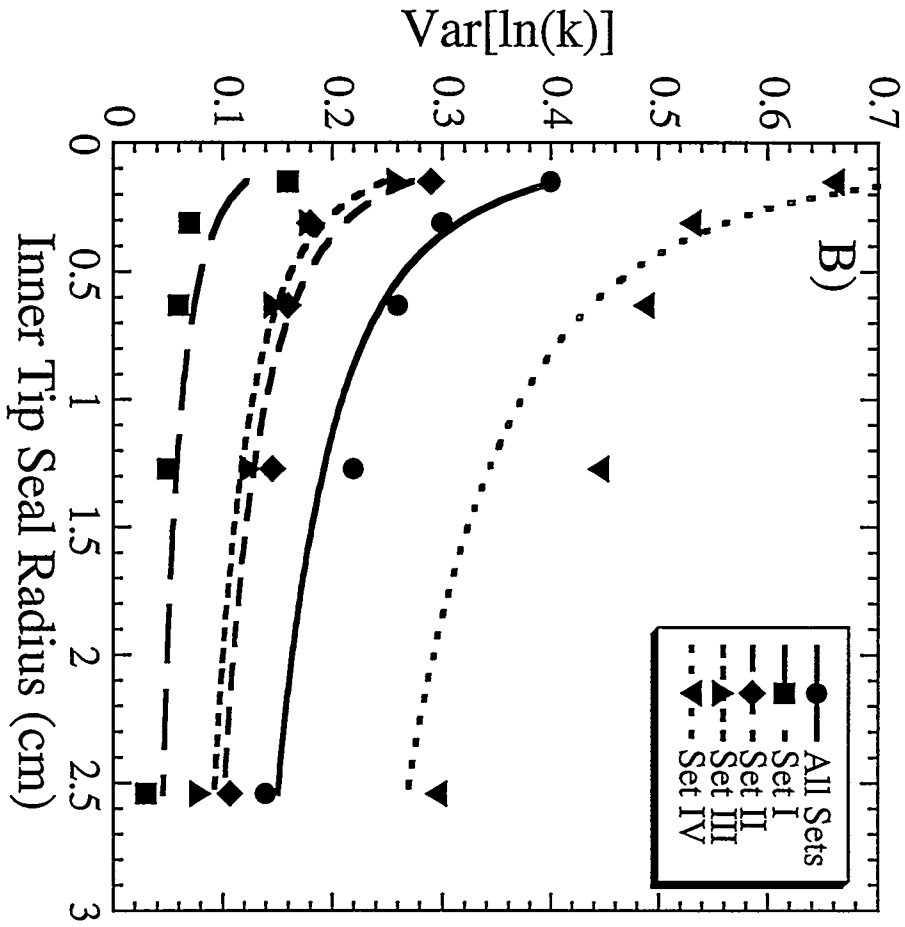
Var[ln(k)]
0
0.1
0.2
0.3
0.4
0.5
0.6
0.7
0
0.5
1
1.5
2
2.5
3
Inner Tip Seal Radius (cm)
B)
All Sets
Set I
Set II
Set III
Set IV

FIG. 5a

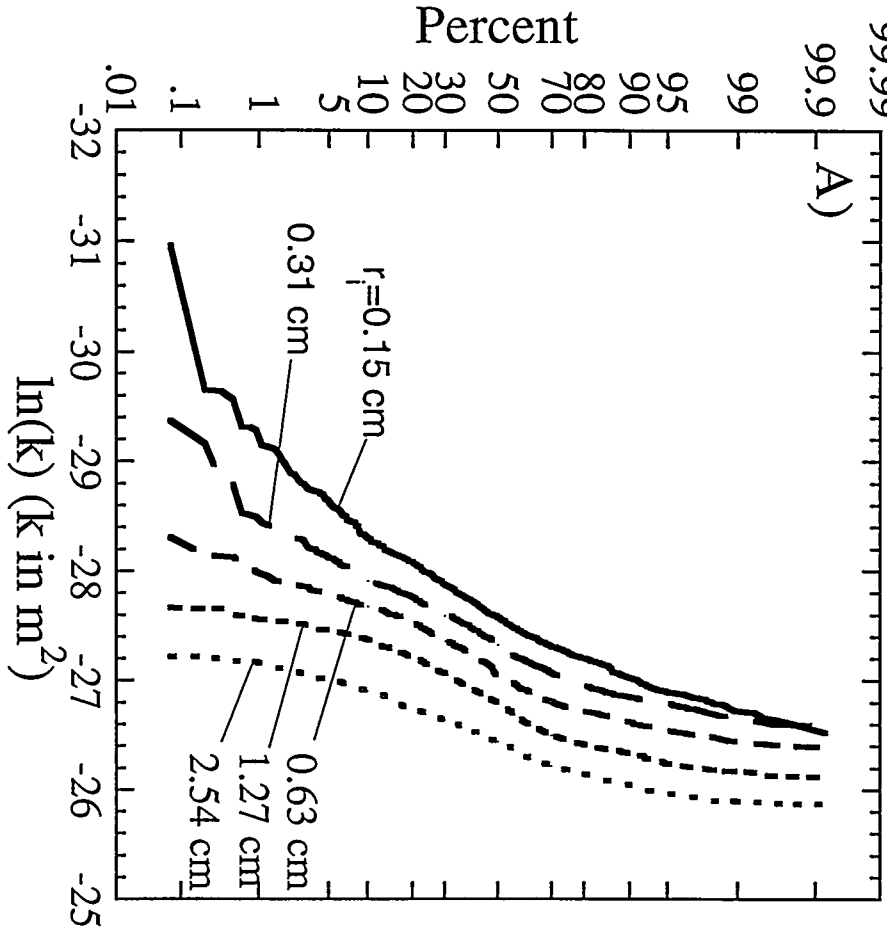
Percent
99.99
99.9
99
95
90
80
70
50
30
20
10
5
1
.1
.01
A)
r_i=0.15 cm
0.31 cm
0.63 cm
1.27 cm
2.54 cm
-32
-31
-30
-29
-28
-27
-26
-25
ln(k) (k in m^2)

Fig 5b

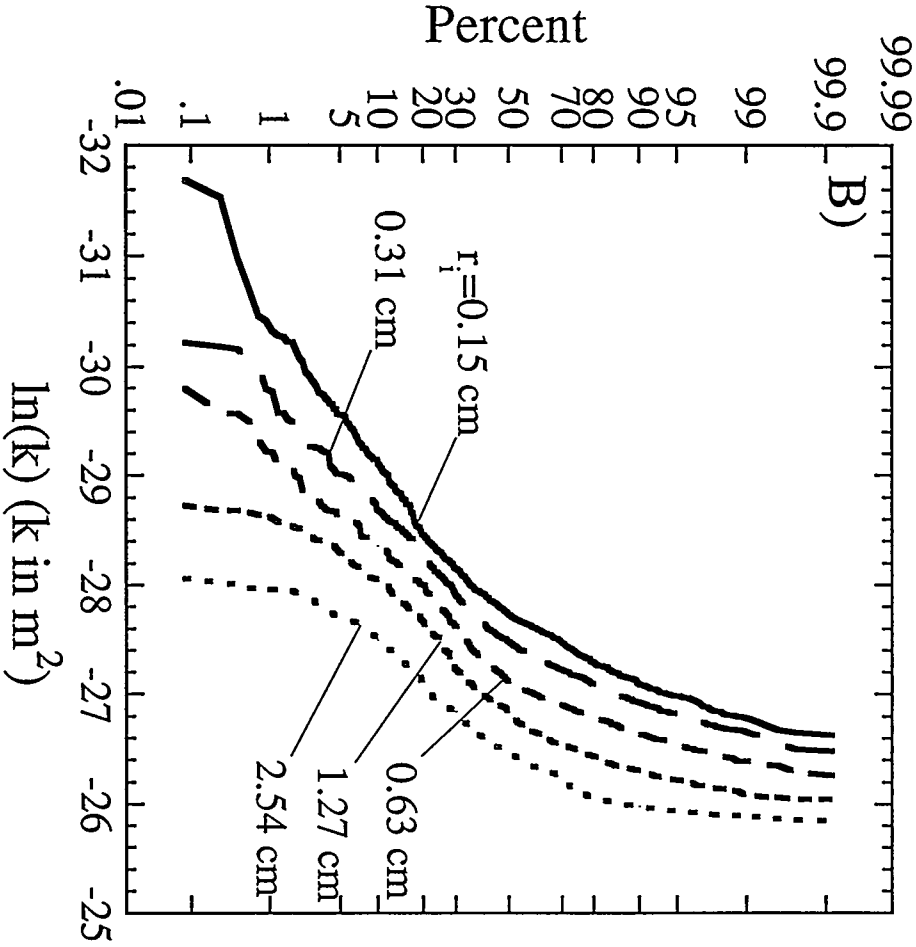
Percent
99.99
99.9
99
95
90
80
70
50
30
20
10
5
1
.1
.01
B)
r_i=0.15 cm
0.31 cm
0.63 cm
1.27 cm
2.54 cm
-32
-31
-30
-29
-28
-27
-26
-25
ln(k) (k in m^2)

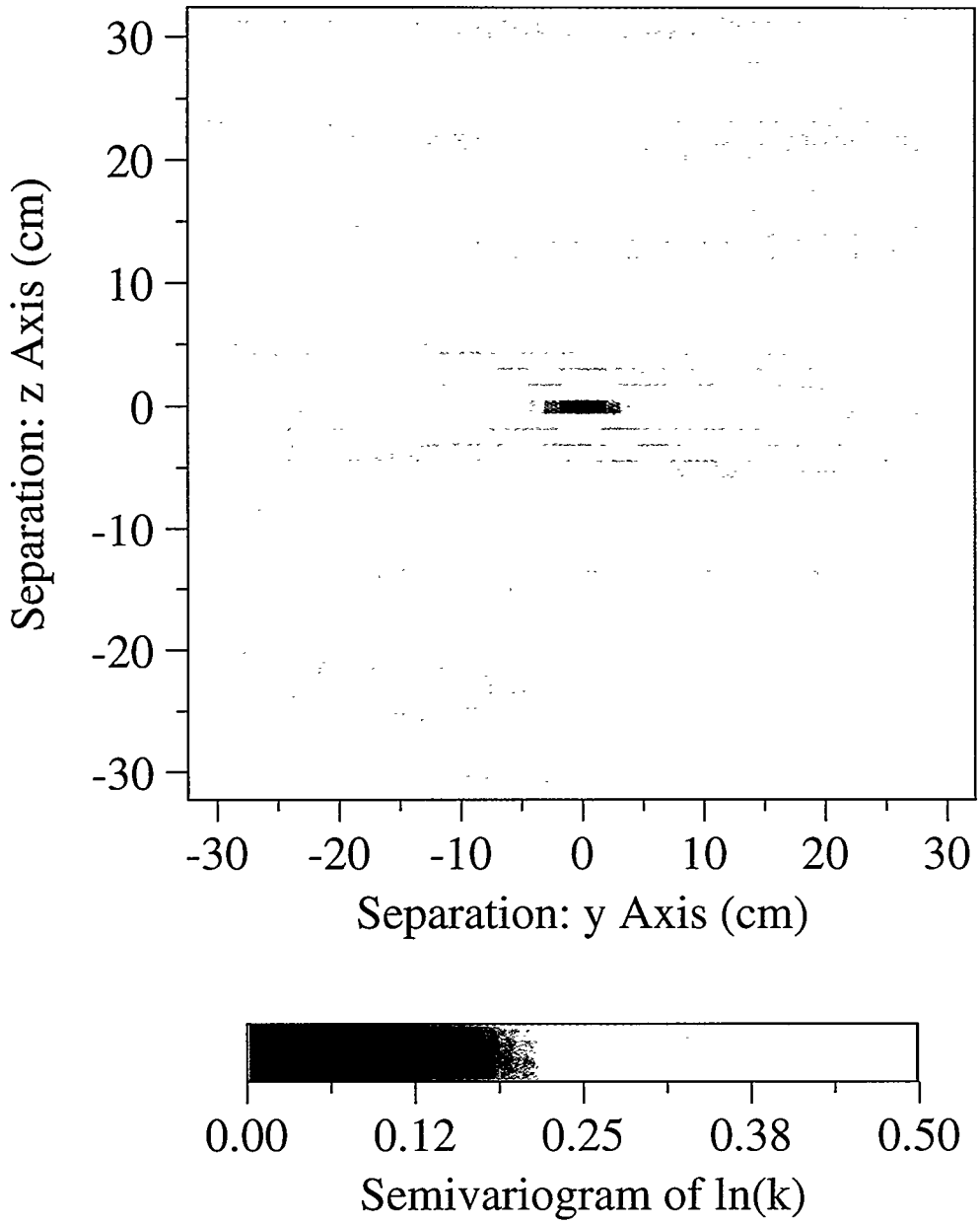
30
20
10
0
-10
-20
-30
Separation: z Axis (cm)
-30
-20
-10
0
10
20
30
Separation: y Axis (cm)
0.00
0.12
0.25
0.38
0.50
Semivariogram of ln(k)

Fig 7a

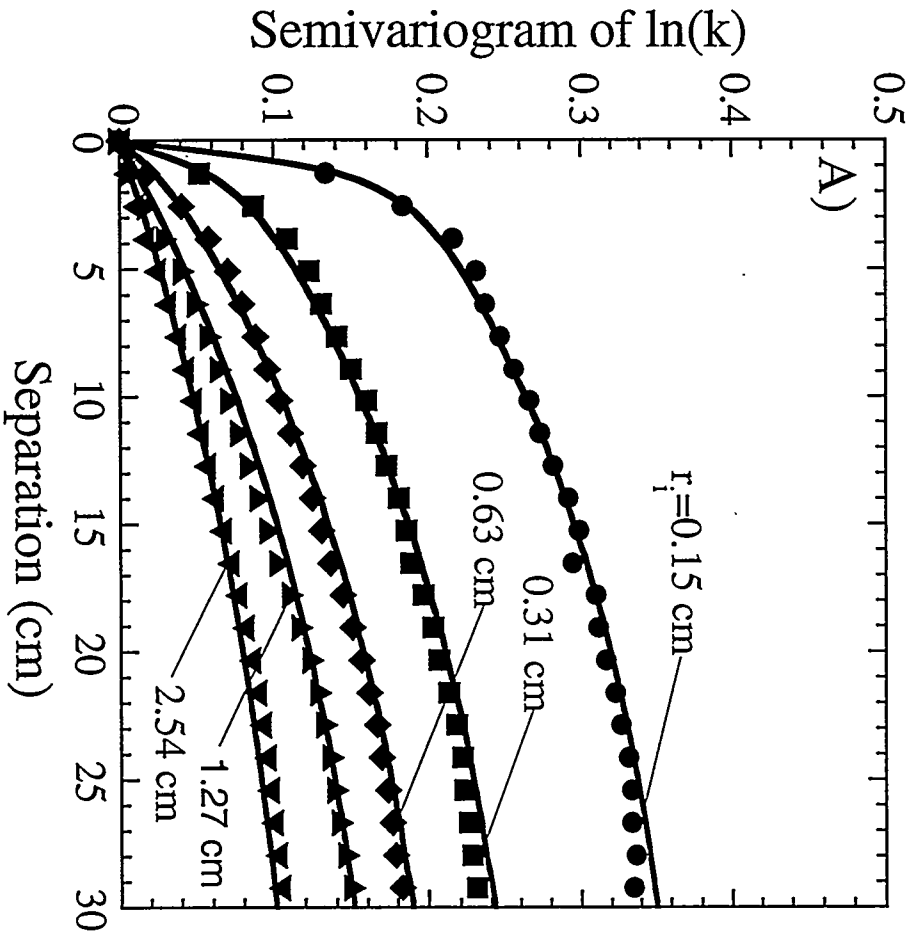
Semivariogram of ln(k)
A)
r_i=0.15 cm
0.31 cm
0.63 cm
1.27 cm
2.54 cm
Separation (cm)
0
0.1
0.2
0.3
0.4
0.5
0
5
10
15
20
25
30

FIG 7b

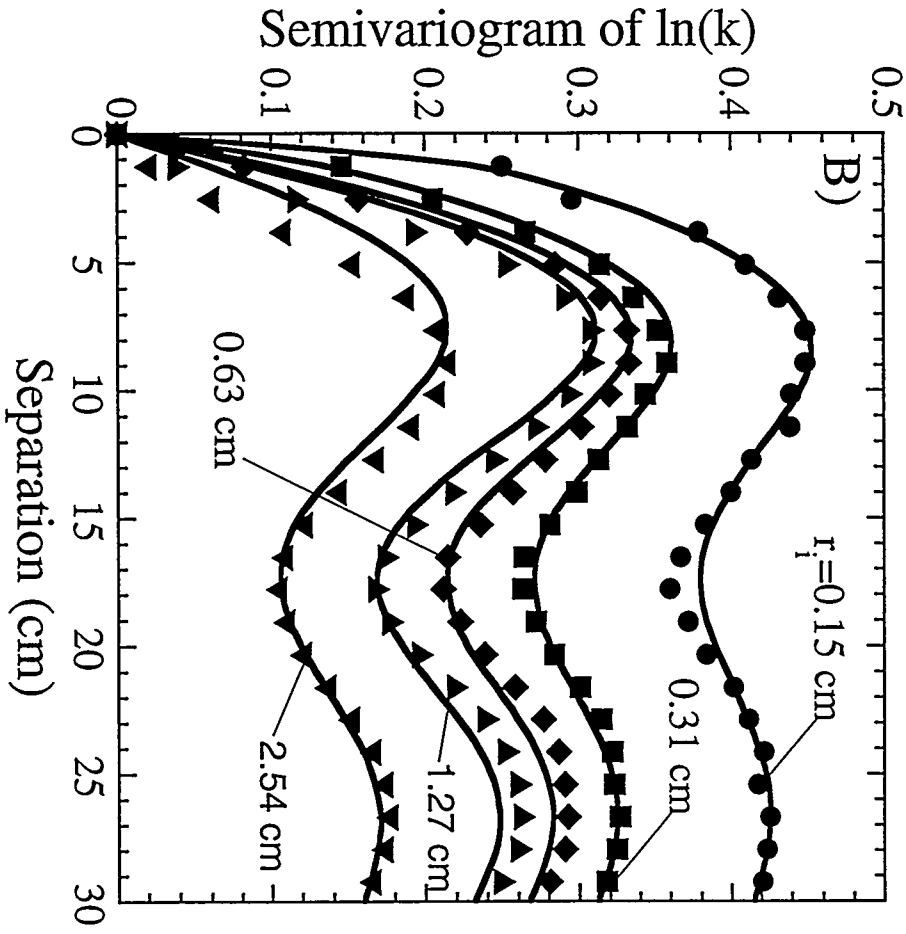
Semivariogram of ln(k)
B)
r_i=0.15 cm
0.31 cm
0.63 cm
1.27 cm
2.54 cm
Separation (cm)
0
0.1
0.2
0.3
0.4
0.5
0
5
10
15
20
25
30

FIG. 8

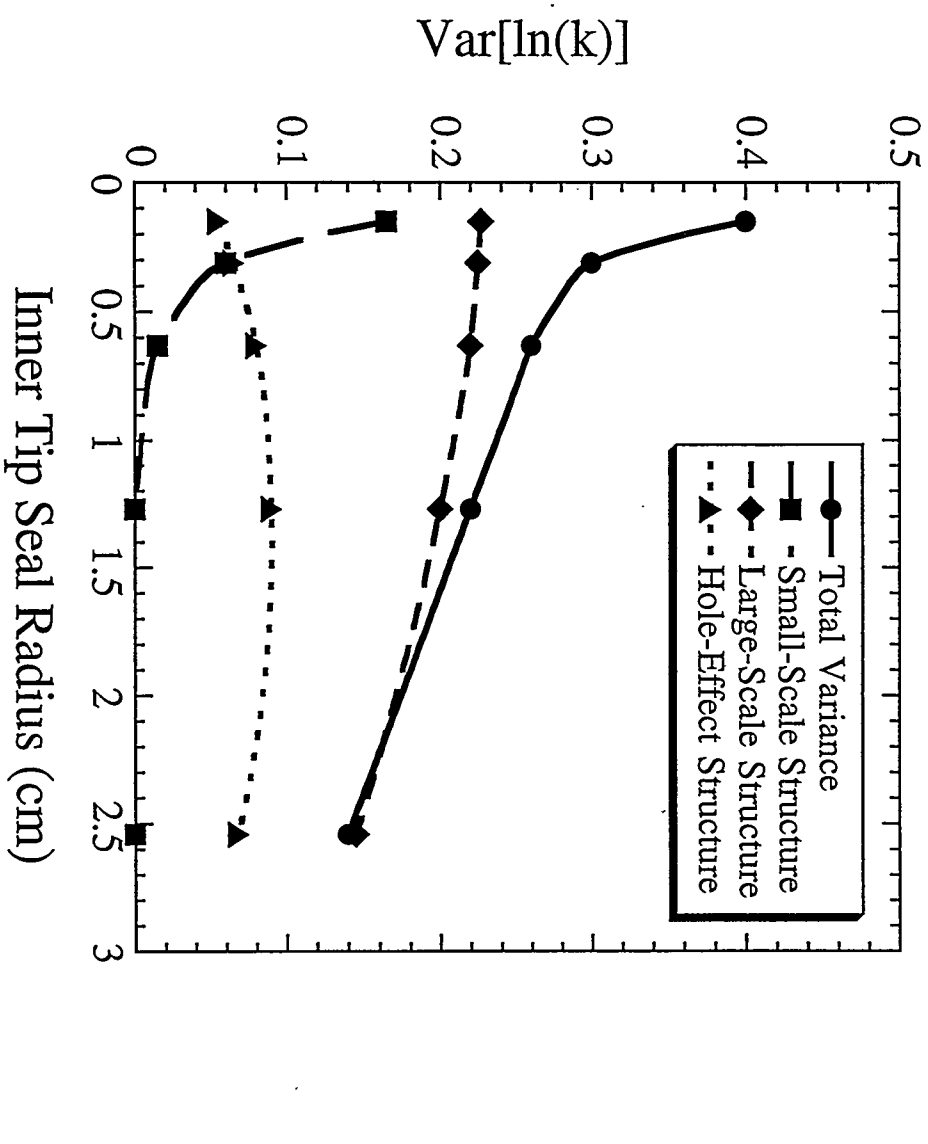
Var[ln(k)]
0.5
0.4
0.3
0.2
0.1
0
0
0.5
1
1.5
2
2.5
3
Inner Tip Seal Radius (cm)
Total Variance
Small-Scale Structure
Large-Scale Structure
Hole-Effect Structure

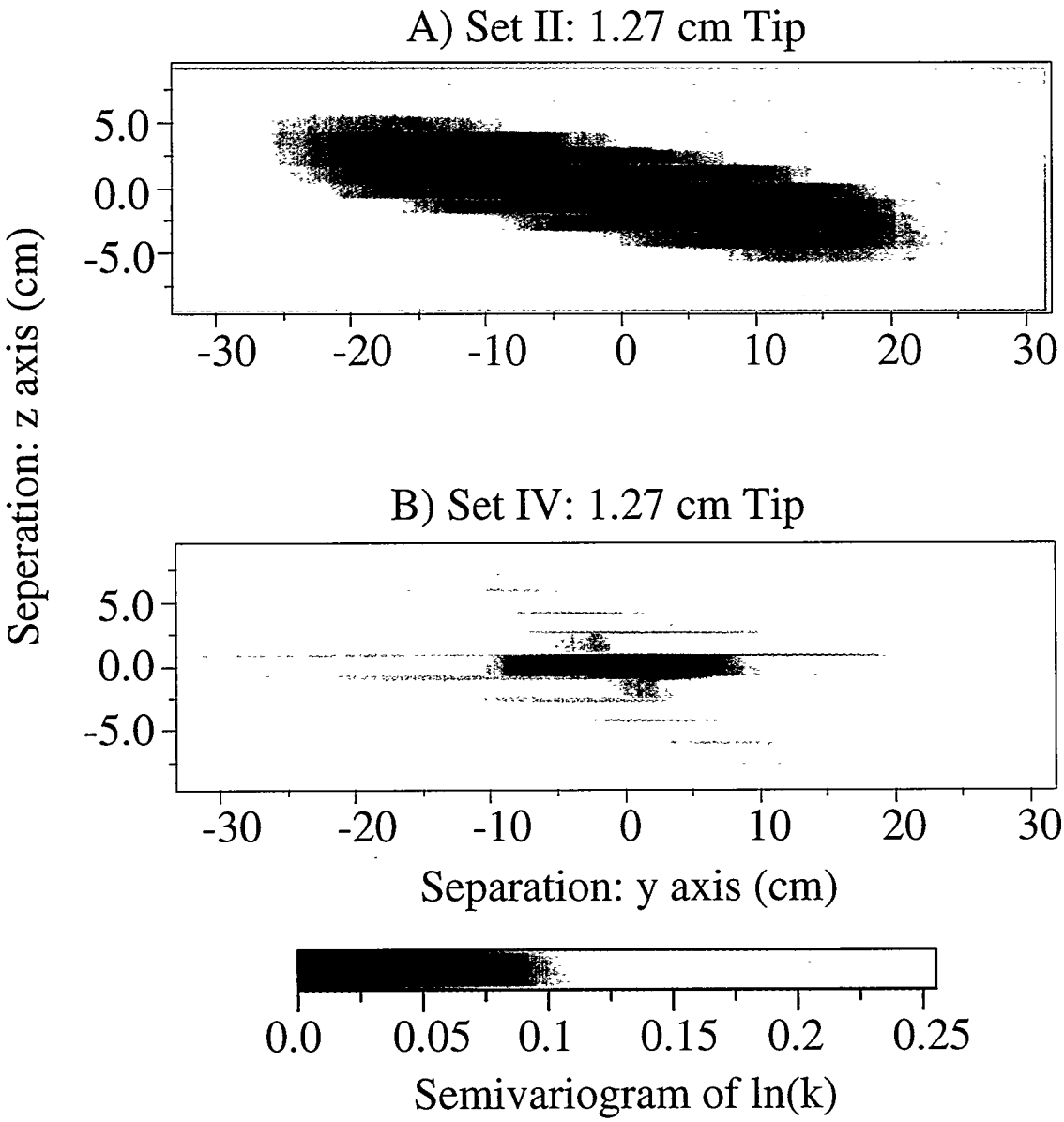
A) Set II: 1.27 cm Tip
B) Set IV: 1.27 cm Tip
Seperation: z axis (cm)
5.0
0.0
-5.0
-30
-20
-10
0
10
20
30
Separation: y axis (cm)
0.0
0.05
0.1
0.15
0.2
0.25
Semivariogram of ln(k)